

**Microstructure and cavitation erosion resistance of some high  
alloyed steels, cast in parts**

**Doctoral Thesis - Abstract**

for obtaining the scientific title of doctor at the Politehnica University of  
Timișoara  
in the PhD field Materials Engineering

**Author eng. Cosma (Alexa) Daniela**

**Scientific leaders: Prof.univ.dr.ing. Ion MITELEA**  
**Prof.univ.dr.ing. Ilare BORDEAȘU**

Timișoara

Month October, Year 2024

## CONTENT

### **Cap.1 Current state of research on cast stainless steels**

- 1.1 The importance of stainless steels*
- 1.2 Classification of stainless steels*
  - 1.2.1 Austenitic stainless steels*
  - 1.2.2 Ferritics stainless steels*
  - 1.2.3 Martensitics stainless steels*
  - 1.2.4 Duplex stainless steels*
  - 1.2.5 Precipitation hardened stainless steels*
- 1.3 The effect of alloying elements in stainless steels*
- 1.4 Cast stainless steels*
  - 1.4.1 Cast stainless steel types*
    - 1.4.1.1 Austenitic stainless steel casting*
    - 1.4.1.2 Ferritic stainless steel casting*
    - 1.4.1.3 Martensitic stainless steel casting*
    - 1.4.1.4 Duplex stainless steel casting*
  - 1.4.2 Stainless steel casting process*
  - 1.4.3 The advantages of stainless steel casting*
- 1.5 Cavitation corrosion*
  - 1.5.1 Description of the cavity corrosion phenomenon*
  - 1.5.2 Previous studies on improving the cavitation corrosion resistance of some cast stainless steels*
- 1.6 The objectives of the doctoral thesis*
- 1.7 Conclusions*

### **Cap.2 Homogenization annealing effect on cavitation resistance of steel GX40CrNiSi25-20**

- 2.1 Introduction*
- 2.2 Chemical composition, microstructure and mechanical properties of the investigated steel*
- 2.3 Cavitation curves*
- 2.4 Microscopic examinations*
- 2.5 Conclusions*

### **Cap.3 Process parameters microstructure and cavitation erosion behavior of remelted TIG surface layers of steel GX40CrNiSi25-20**

- 3.1 Introduction*
- 3.2 Principle of the method. Process parameters*
- 3.3 Hardness tests*
- 3.4 The microstructure of the composite system: layer remelted- substrate*
- 3.5 Cavitation curves*
- 3.6 Macro and micrographic of sections through remelted layers, cavitation tested*
- 3.7 X-ray diffraction analysis*
- 3.8 Topography of surfaces eroded by cavitation*
- 3.9 Conclusions*

**Cap.4 Process parameters, microstructure and cavitation erosion behavior of laser remelted surface layers of steel GX40CrNiSi25-20**

*4.1 Introduction*

*4.2 Materials and experimental procedure*

*4.3 Evaluation and interpretation of experimental results*

*4.3.1 Hardness tests*

*4.3.2 Specific curves and characteristic parameters of cavitation erosion*

*4.3.3 Structural changes*

*4.4 X-ray diffraction analysis*

*4.5 Conclusions*

**Cap.5 Microstructure and cavitation resistance on weld deposited layers of manganese austenitic alloy**

*5.1 Introduction*

*5.2 Materials, experimental procedure*

*5.3 Structural analyses*

*5.4 Cavitation curves*

*5.5 Comparison between the 3 samples coated with manganese austenitic steel and comparison with the initial steel GX40CrNiSi25-20 in the annealed state*

*5.6 Conclusions*

**Cap.6 Final conclusions and original contributions. New research directions**

*6.1 Final conclusions and original contributions*

*6.2 New research directions*

**Bibliography**

## Introduction

Cavitation erosion is one of the three effects of cavitation. It occurs as a result of the impact of the surface with shock waves and microjets generated by the rapid implosion of bubbles filled with gases and/or vapors at high pressures.

This erosion phenomenon causes changes in geometry, modification of the surface structure, this leads to the total or partial change of the damaged components.

In Romania, the best-known laboratory for studying/researching cavitation erosion is the Cavitation Erosion Research Laboratory from the Politehnica University of Timișoara, which has research activity for over 60 years.

By purpose and objectives, the PhD thesis highlights the behavior and resistance to cavitation of cast stainless steel GX40CrNiSi25-20 parts. The content of the thesis is structured in 6 chapters as follows: the first one is intended to present, succinctly, the state of the fields of use of stainless steels; the second one is intended to present the effect of homogenization annealing on the cavitation resistance of GX40CrNiSi25-20 steel, the third one is intended to present how the Wig remelted surface layers of GX40CrNiSi25- steel grade behave to cavitation erosion 20.

The fourth one is intended to show how the laser remelted surface layers of the GX40CrNiSi25-20 steel brand behave to cavitation erosion. The fifth chapter covers the microstructure and cavitation resistance of the layers deposited by welding of manganese austenitic alloy over the surface of the analyzed steel.

The last chapter is intended for the synthesis of general conclusions, personal contributions and the description of future research directions.

The results of this thesis are a continuation of those achieved in the Cavitation Erosion Research Laboratory of the Politehnica University of Timișoara, they are on the wave of current research on the creation of stainless steel surface structures cast in pieces, which can satisfy the requirements of operation in cavitation conditions with low and medium intensity and is the basis for future research, on other categories stainless steel cast in pieces.

### Cap.1 Current state of research on cast stainless steels

Their symbolization is done according to SR EN 10027 – 1:1996.

Example: Ex. G X3CrNi 18-8:

where: G symbolizes cast steels; 3 represents the carbon content in hundredths of percent; 18 percent of Cr; 8 percent of Ni.

Cast stainless steels are generally classified according to alloying element content and intended use into the categories: corrosion-resistant steels and heat-resistant steels. Steel castings are classified as corrosion resistant if they are capable of sustained service when exposed to attack by corrosive agents at service temperatures that are generally below 300°C.

The usual distinction between heat-resistant and corrosion-resistant cast steels is based on carbon content.

A significant difference between cast and forged stainless steels lies in the microstructure of cast stainless steels. There is usually a small amount of ferrite present in austenitic stainless steel castings, in contrast to the single-phase austenitic structure of wrought alloys [43][61].

Wrought and cast stainless steels can also differ in mechanical properties, magnetic properties and chemical composition. Due to the possible existence of large dendritic grains, intergranular phases and segregation of alloying elements, the typical mechanical properties of cast steels can vary more and are generally inferior to those of any forged structure[69].

In cast steels, corrosion resistance is largely dependent on the absence of carbon, and especially precipitated carbides, in the microstructure of the alloy. Therefore, corrosion-resistant cast alloys are generally low in carbon (typically less than 0.20% and sometimes less than 0.03%) [97].

All cast corrosion-resistant steels contain more than 11% chromium and most contain from 1 to 30% nickel (a few have less than 1% Ni) [17].

Cast stainless steel structures can be austenitic, ferritic, martensitic or ferrite-austenitic (duplex) [90]. The structure of a particular brand is mainly determined by its chemical composition. Chromium, molybdenum and silicon promote the formation of ferrite (magnetic), while carbon, nickel, nitrogen and manganese promote the formation of austenite (non-magnetic).

Chromium (a ferrite and martensite promoter), nickel and carbon (austenite promoters) are particularly important in determining the microstructure.

In general, stainless steels with the main alloying element chromium are either martensitic or ferritic, chromium-nickel steel grades are either duplex or austenitic, and nickel-chromium steels are fully austenitic [98].

#### *Previous studies on the improvement of cavitation corrosion resistance of some cast stainless steels*

Inside the moving liquid there is a tendency to form bubbles filled with gas vapors. Bubbles formed in the moving liquid develop, become nearly spherical and can be transported to a region of higher pressure than the vaporization pressure. There is then a sudden breaking of the walls of the bubbles towards their interior, a process called implosion and which is accompanied by a complex of physical and chemical phenomena that lead to cavitation erosion of the material of the components that are exploited in such an environment [126].

The implosion is primarily accompanied by the appearance of very high pressures that have important effects on the material walls that border the moving fluid. If the implosion occurs near a wall, the pressure is exerted directly on it; if the implosion occurs at some distance from the wall, the pressure is transmitted in the form of pressure waves. The mechanical effects of the implosion are extremely strong, which also results from the fact that no currently known material resists cavitation [116].

In addition to the mechanical phenomena, which are predominant, in the case of implosion, there are also thermal phenomena, mainly due to the behavior of the gas in the bubbles, as well as chemical phenomena, due to the formation of corrosive chemical substances. Even electrical phenomena were observed. Cavitation is always accompanied by loud noises and vibrations. The solid surfaces located in the area where the implosions occurred show, after a while, erosion phenomena in the form of caverns, of irregular outline and depth. The destruction of a solid surface due to cavitation is called cavitation erosion (corrosion) [29].

At first, sliding and plastic deformations occur in the superficial layers, then at the base of the irregularities cracks are initiated which gradually propagate in the superficial layer of the material. As a result of the research, it turned out that the mechanism of cavitation erosion and the destruction of the material is also related to the chemical composition of the environment. These non-mechanical factors can greatly accelerate the destruction process. An important role in the intensity of destruction is played by the chemical and electrochemical reactions of the metal with the working environment. For example, sea water, in any metal, produces an increase in the cavity compared to fresh water.

Cavitation corrosion occurs in installations such as hydraulic turbines, pump impellers, turbochargers, control valves and other hydrodynamic elements.

Hydrodynamic systems are manufactured with materials resistant to corrosion and mechanical damage. In terms of material selection, it should be noted that ductile materials are stronger than brittle materials, materials with higher fatigue resistance also have greater resistance to cavitation erosion. At the same time, the resistance to cavitation increases with the decrease in the size of the crystalline grains of the materials.

The hardening of the superficial layer by classical thermal treatments, by laser beam hardening or ion implantation, leads to the increase of approximately 2-3 times the incubation period of cavitation, thus delaying its appearance. Materials with a crystalline structure with centered faces are isotropic and little sensitive to the increase of the deformation speed [65][66].

Finding some materials that have a low cost price and high resistance to cavitation erosion, led to the creation of laboratory facilities, which allow a more systematic analysis of the behavior of materials to cavitation attack. The big disadvantage of these installations is the cavitation attack duration, which must be very long for materials with fine structures and high mechanical characteristics, such as stainless steels [58]. However, this disadvantage is eliminated by vibratory devices which present the disadvantage of creating a cavitation process totally different from the real one (from the industrial machine).

The evaluation of the behavior of the materials, respectively the estimation of their resistance to cavitation erosion is done on the basis of the characteristic curves or the values of the various parameters. The ordering and evaluation of the resistance of materials to cavitation erosion is done according to one of the criteria:

- a. the slope of the mass  $m(t)$ , volume  $V(t)$  or gravimetric loss curves in the stabilization zone,  $\text{tg}\alpha$ , [28][65][66];
- b. the value towards which the cavitation erosion speed tends to stabilize,  $v_s$ , [57], [58][61],
- c. the maximum value of the cavitation erosion speed,  $v_{\text{max}}$  [57][58],
- d. the normalized resistance to cavitation  $R_n$  [57],
- e. the speed of the average or maximum erosion penetration depth, MDPR respectively MDPRmax, (or their inverse  $1/\text{MDPR}$ , respectively  $1/\text{MDPRmax}$ .) [57][65][66],
- f. incubation time,  $t_i$ , [28][47],
- g. the time required to achieve a given volume or mass loss [12][28],
- h. the time required to achieve a certain depth of penetration [28][48].

Figure 1.1 shows the characteristic curves and the above-mentioned indicators, defined by these curves. Since the experimental results are influenced by the technical-functional parameters of the station, allowing a degree of subjectivity, at the current stage there is no resistance estimation method unanimously accepted by cavitation specialists [41][47].

ASTM norms [12] recommend parameters 1, 2, 3 and 4, and Thiruvengadam [166] recommends erosion stabilization rate. For the maximum speed of cavitation erosion, the ASTM norms [12] recommend that value after which the speed becomes decreasing. This recommendation is made because the high values, in the first minutes of the cavitation attack, (obtained mainly in vibratory devices) are strongly affected by the abrasive dust and the level of roughness in the attacked surface [56].

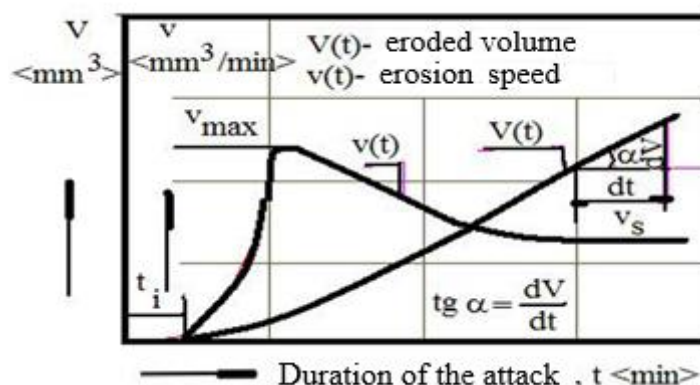


**Figure 1.1** Curves and characteristic quantities used in the estimation of cavitation erosion behavior and resistance [28]

Cavitation erosion is a complex and localized phenomenon involving mechanical, chemical and metallurgical parameters. The development of new materials depends on understanding the relationship between microstructure and cavitation erosion. When subjected to cavitation erosion, materials behave differently depending on their chemical composition, microstructure, surface treatments, etc. [69].

During cavitation erosion of metals and alloys, the mechanical hardening process due to the collapse of bubbles in the surface layer of the part is associated with an increase in hardness

[52]. It was also observed that in ductile materials, the cavitation erosion rate is influenced by the ratio between the thickness of the hardened layers at the time of coating, and the speed of the flow [54].

The ultrasonic test method [37] leads to the formation of a cloud of cavitation bubbles, almost uniform in their shape, obtained at a fixed frequency, compared to real cases where there is a distribution of different sizes as well as different frequencies. The standardized test does not allow a complete characterization of the behavior under real conditions due to the absence of a real liquid flow or the interaction of bubble nuclei with turbulent vortex filaments.

Compared to the actual cavitation erosion that occurs after a long period of exposure, standardized accelerated tests performed in the laboratory can be used to compare materials tested under similar conditions. The equipment for this purpose conducts an intensive erosion process in a controllable and reproducible way, by generating clouds of bubbles that erode the surface of a sample made of the tested material. Such equipment can be used to evaluate the cavitation erosion resistance of a material in terms of erosion rate, thus allowing a classification of materials based on this property.

In order to evaluate the erosion process, ultrasonic equipment is used, according to the standards, ASTM G32-2016 [13]. They have the advantage that easily controllable parameters can be established, which generate longitudinal vibrations, amplified and transmitted in the liquid as ultrasonic waves. The bubbles that form during these vibrations cause implosions on the surface of the samples and generate a destructive effect on the surface with an energy that depends on the parameters used in the process and the characteristics of the ultrasonic probe. Cavitation erosion pinches depend on the particularities of the material's behavior in the fatigue phenomenon [6].

An increase in liquid viscosity is predicted to lead to reduced surface erosion as a result of decreasing bubble growth and collapse rates [134].

Cast stainless steels are classified as "corrosion resistant" when used in aqueous and vapor environments below 650°C and "heat resistant" when used above this temperature [114]. The usual distinction between grades of heat-resistant and corrosion-resistant cast steels is given by the carbon content.

Heat-resistant steel grades have high carbon contents to improve resistance at high temperatures [69]. Chemical composition and microstructural differences between rolled and cast versions of stainless steels can affect their performance. Although some grades of cast stainless steels can be hardened by solution quenching heat treatment followed by temper aging, the mechanical properties of most of these alloys are based on their chemical composition [52].

Cast stainless steels have similar corrosion resistance to their as-rolled equivalents, but may become less corrosion resistant through cavitation erosion due to localized contamination, microsegregation or inhomogeneity [69]. For example, mold quality can cause superficial compositional changes that influence performance, and carbon uptake from mold release agents can affect corrosion and cavitation erosion resistance [116].

The researches carried out show that all materials used in the manufacture of valves that are part of the flow path, working under the same conditions, are subject to cavitation erosion, in different proportions. The most significant erosive destruction occurs when they are made of carbon and low-alloy steels. Conversely, for similar operating conditions, stainless steels (containing chromium, chromium-nickel, etc.) have higher cavitation resistance.

Because, the metallic materials subjected to cavitation attacks are, in general, alloys obtained from the combination of several metals with different crystal lattices (hexagonal compact (HC), volume-centered cubic (CVC), face-centered cubic (CFC), etc.), for understanding of the mechanism of erosion, research was carried out on both pure metals and alloys. For a clearer understanding, the erosion process was followed both during the incubation period and during the advanced erosion period.

Heathcock et al. [74] studied the erosion mechanisms of several types of materials such as: pure iron, ferritic stainless steels, cobalt, nickel alloys and some polymers. Their studies refer to materials that have been subjected to cavitation in rotating disk machines,

hydrodynamic tunnels and industrial machines, where there is an incubation period of erosion [37]. They believe that during the incubation period only plastic deformations and the formation of microcrack networks (a phenomenon observed by all researchers), associated with the phenomenon of fatigue due to the cyclical contractions that occur during the cavitation attack, take place. After this period, they observed that material losses are caused by ductile or brittle fractures through the propagation of already existing cracks, simultaneously with local fatigue cracking [54].

The studies carried out by Heathcock [74] on the austenitic stainless steels AISI 409, AISI 430, show that the poor resistance to cavitation erosion is determined by the sensitivity of the materials to the strain rate. Thus, it is demonstrated that the high deformation speed, typical of cavitation, leads to a brittle fracture in the attacked surface. At the same time, it was observed that the material whose cavitation breakage was less fragile, contained the lowest percentage of chromium.

Heathcock's conclusions [74] were also reached by Binder and Spendelow [22] who, in addition, showed that the synergistic effect of the presence of chromium, in particular for concentrations of 15-18%, combined with the critical concentrations of carbon and nitrogen accentuates the sensitivity on the strain rate of metals with a volume-centered cubic crystal lattice. The authors observed that while the erosion mode of steel with a ferritic structure is almost entirely brittle, the alloys that have a fine structure become more ductile and more resistant to cavitation attack, with the increase in the percentage of martensite volume fraction [74].

### ***The objectives of the thesis***

The research program aims to deepen the degradation mechanism and establish the ways of increasing the cavitation erosion resistance of cast stainless steels by applying some surface ennobling techniques.

The experiments aim to find a correlation between the structural state of the material and the speed of degradation through cavitation erosion, as well as the optimization of the technological processing process in order to increase the life of the engineering components that work in such conditions.

It is estimated that by applying some techniques of physical modification of the surface, to obtain a layer-substrate compound system that responds favorably to the exploitation of oligocyclic stresses (the field of low durability or oligocyclic fatigue), in cavitation environments.

The development of methods for testing cavitationally degraded surfaces will allow a more precise control of the evolution of this phenomenon with implications in reducing the risk of damage.

The main processes that are considered to have a positive impact in ensuring an increase in cavitation resistance are:

- applying a heat treatment after the casting operation;
- WIG or laser beam remelting of the surface layer;
- depositing layers of manganese austenitic steel on the surface using the TIG welding technique.

The assessment of the quality of the cavitationally tested surface is done by:

- ✓ macro- and microscopic investigations;
- ✓ sclerometric examinations;
- ✓ microfractographic analyzes with the scanning electron microscope;
- ✓ EDX and X-ray diffraction analyses.

### ***The novelty of the doctoral thesis***

The novelty of the doctoral thesis consists in the phenomenological deepening of erosion by cavitation and the definition of methods of ennobling the surface of cast stainless steel parts in order to increase the life of the equipment working in such conditions.

## Cap.2 Effect of homogenization annealing on cavitation resistance of GX40CrNiSi25-20 steel

GX40CrNiSi25-20 is a cast steel, used for the manufacture of elements used at high mechanical stress and for cavitation or high temperature working environments [23][152]. Its resistance to cavitation erosion is relatively low and limits its use in intense cavitation environments.

Areas of use:

- Automotive industry: (turbochargers, manifolds, valves, )
- Mechanical engineering: (flow elements, parts for hot gas flow ranges 900-1100°C)
- Installation engineering: (for oil and gas, valve bodies)
- Heavy industry: parts subject to high stresses (conveyor rolls, radiant tube heaters, centrifugal casting pipes)

Classification of GX40CrNiSi25-20 steel, with 25% chromium and 20% nickel content (Table 2.1):

**Table 2.1** Classification of steel GX40CrNiSi25-20[122]

Name	GX40CrNiSi25-20
Number	1.4848
Classification	Austenitic cast steel resistant to high temperatures
Density	7,8 g/cm <sup>3</sup>
Standard	EN10295:2002

Chemical composition % of steel GX40CrNiSi25-20 (1.4848): EN 10295-2002 (Table 2.2)

**Table 2.2** Chemical composition,%, of steel GX40 CrNiSi25-20 [122]

C	Si	Mn	Ni	P	S	Cr	Mo	Fe
0,3-0,5	1-2,5	max. 2	19-22	max.0,04	max. 0,03	24-27	max.0,5	45-55

From steel GX40CrNiSi25-20 (W.1.4848), EN 10295, having the chemical composition: C = 0,38%, Cr = 25,20%, Ni = 20,8%, Si = 1,62%, Mn = 1,49%, Mo = 0,34%, P = 0,031 %, S = 0,027 %, cylindrical samples Ø 25 x 40 mm were taken. They were subjected to the heat treatment of annealing for homogenization at T = 1100 °C, for 8 h, cooling in the oven. After this volumetric heat treatment, samples were prepared for the cavitation tests (Figure 2.1).

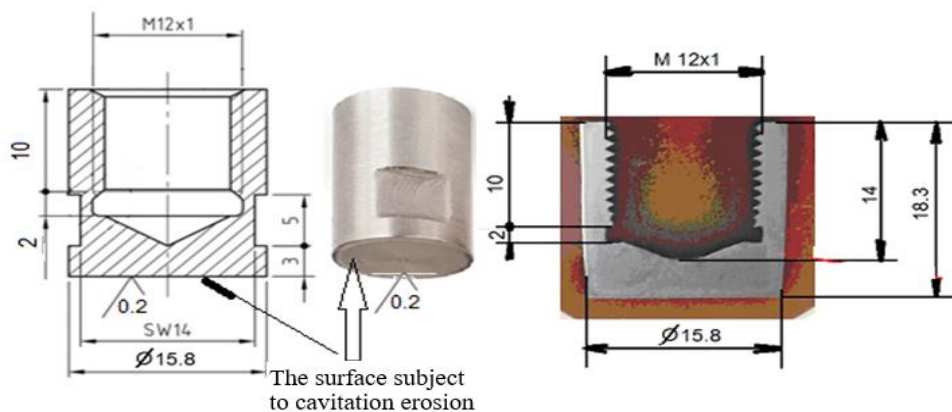


**Figure. 2.1** Cavitation test

The experimental researches were carried out in the cavitation laboratory in Timișoara, Politehnica University, on the vibrating device with piezoceramic crystals (Figure 2.2), which is controlled by a computer and equipped with an automatic command of the functional parameters that define the hydrodynamic process of cavitation.

This type of device allows the testing of different types of materials at intense cavitation, thus considerably reducing the duration of the attack of the samples, compared to the existing situations in real life or when other methods of generating the cavitation phenomenon are used (the case of the hydrodynamic tunnel [29] or of rotating disc device [21–23]).

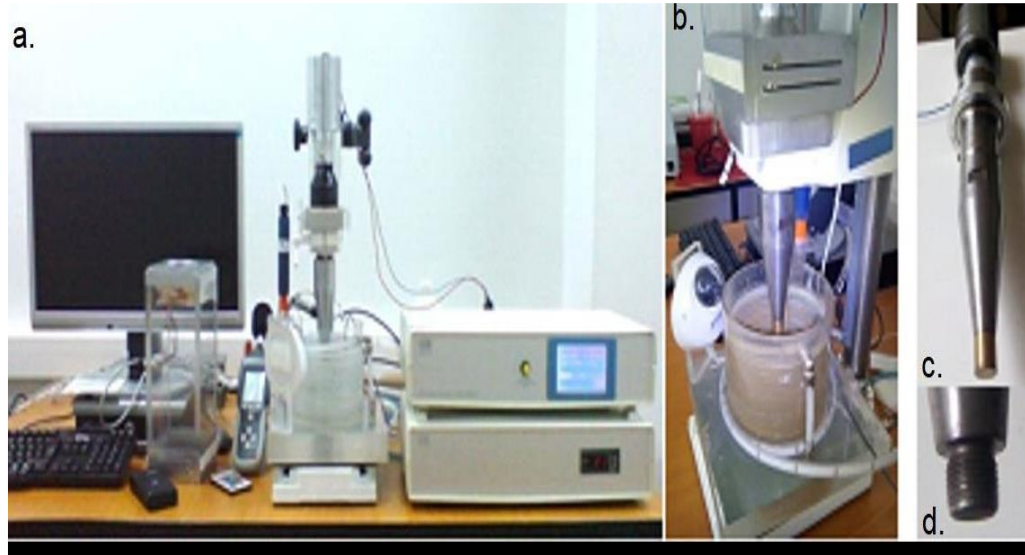


**Figure 2.2** The vibrating device with piezoceramic crystals: a. overview of the device with the computer control system; b. image during the cavitation test (sample immersed in water); c. mechanical vibration system (piezoceramic transducer with amplitude amplification system (buster, sonotrode and cavitation sample)); d. threaded end of the sonotrode for fixing the sample

The functional parameters of the device are:

- the power of the electronic ultrasound generator, 500 W;
- vibration frequency,  $20000 \pm 2\%$  Hz;
- vibration amplitude, 50  $\mu\text{m}$ ;
- sample diameter:  $15,9 \pm 0,05$  mm;
- power supply: 50 Hz;
- liquid: distilled water having a temperature of  $22 \pm 1^\circ\text{C}$

Both at intermediate periods of attack and at the end of the 165 min of cavitation erosion, the surface topography was investigated using both the OLIMPUS SYX7 optical stereomicroscope and the TESCAN VEGA 3 LMU Bruker EDX Quantax scanning electron microscope. Following the cavitation tests, the samples were sectioned and metallographically prepared. Both the Leica DM2700M optical microscope and the scanning electron microscope were used to examine the edge layer where the cracks initiate and then propagate as a result of cavitation.

Cast steel GX10Cr13 (C = 0,11%; Cr = 12,78%; Ni = 1,054%) was used as a reference material, which is intended for the execution of engineering components frequently requested in cavitation environments.

In Figure 2.3 and 2.4, the evolution of the average erosion depth and the average erosion speed can be observed comparatively, for the two brands of steel:

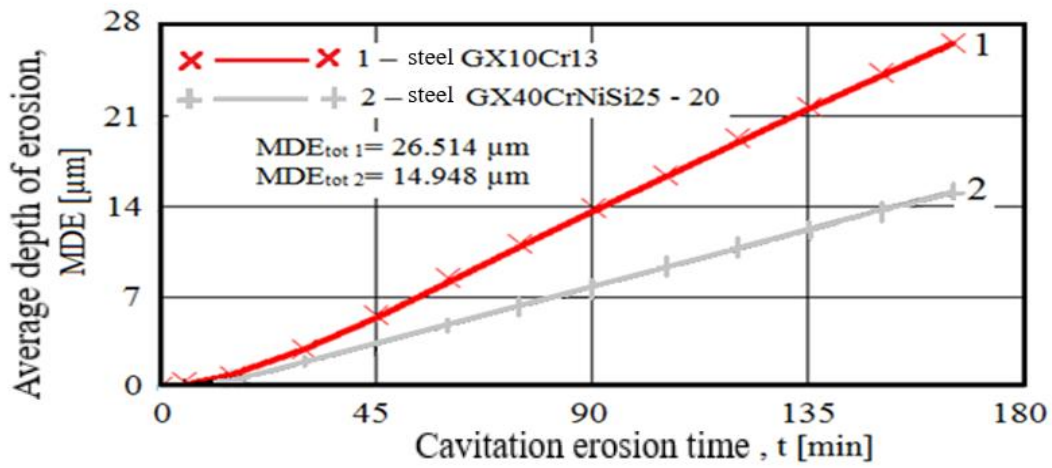


**Figure 2.3** Evolution of the average erosion depth with the duration of the cavitation attack

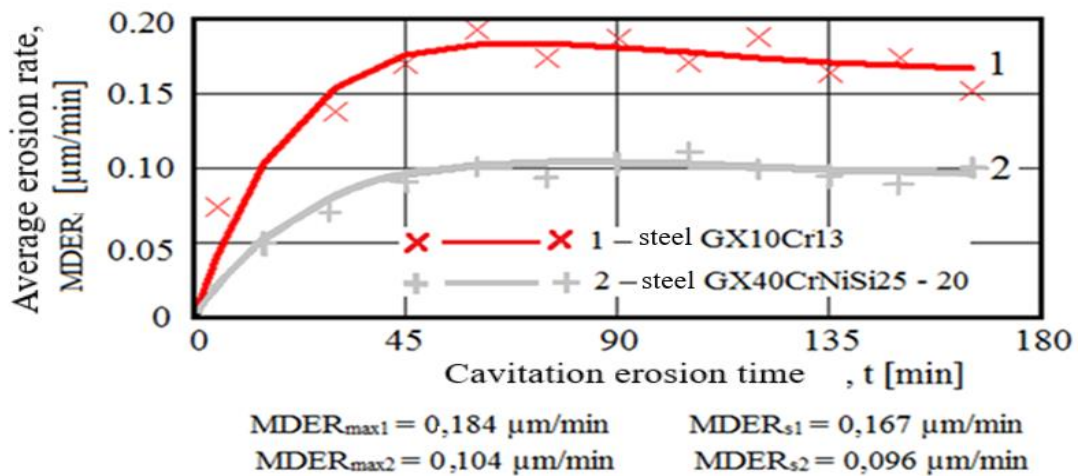


**Figure 2.4** The evolution of the erosion speed with the duration of the cavitation attack

### Conclusions

Compared to the reference steel GX10Cr13, the analyzed steel GX40CrNiSi25-20 provides an increase in cavitation resistance of about 1,8 times after the maximum value of the cumulative average depth of erosion, MDE, respectively about 1,7 times after the values towards which the parameter stabilizes erosion rate, MDER.

Surface damage caused by exposure to cavitation is initiated at the boundaries between the phases, followed by the removal of chemical compounds, subsequently the attack of the austenite matrix occurs.

### Cap.3 Process parameters, microstructure and cavitation erosion behavior of WIG remelted surface layers of GX40CrNiSi25-20 steel

This chapter aims to find a solution to combat cavitation erosion by improving the surface properties of high-alloy steels cast in parts, using the TIG surface modification technique. The TIG process of local surface remelting is simple, flexible and economical, achieving microstructure modification without adding new material.

Following its application, it is expected to obtain a homogenization and a finishing of the microstructure, a dissolution / redistribution of precipitates or inclusions, while the properties of the substrate can be preserved [99][101][102]

The experimental research aimed to study the influence of the linear welding energy on the geometry of the melt, respectively the structural changes in the molten metal compared to the thermally unaffected base metal. The samples (Ø 25 x 40 mm), in number of three, were

made of steel GX40CrNiSi25-20 (W.1.4848), EN 10295. These samples were subjected to heat treatment of annealing for homogenization (at 1100°C/8 hours with cooling in oven). Afterwards, they were TIG remelted using three different thermal regimes. The change in linear energy,  $E_l = (U_a \times I_s) / v \times 60$  [J/cm] was achieved by changing the value of the welding current, keeping the welding speed constant, as shown in Table 3.1:

**Table 3.1** TIG regimes used for remelting steel samples

Regime TIG	Remelting parameters				
	Welding current $I_s$ [A]	Arc voltage $U_a$ [V]	Arc length $l$ [mm]	Welding speed $v$ [cm/min]	Linear energy $E_l$ [J/cm]
1	100	10,2	2	15	4080
2	150	10,5			6300
3	200	11,1			8880

According to technological recommendations, the base material was preheated to a temperature of 250°C and the temperature between passes was maintained at values of 250-300° C

To remelt the surface of the samples, parallel passes were made, with a step between passes equal to two thirds of the width of a pass, so as to create an overlap of the passes of approx. 1/3 of the width of the pass, which allowed to obtain a smooth melted surface without welding defects (lack of melting or marginal notches).

To avoid metal leakage on the circumference of the cavitation samples, they were embedded in a 5 mm thick carbon steel plate. Finally, the cavitation samples were taken from the non-alloy steel plate by water jet cutting.

The depth of the remelted layer was between 1,3 and 2,7 mm, depending on the value of the remelting current.

The front surfaces of the remelted samples with the 3 values of the welding current, respectively of the linear energy, were processed by the grinding operation and then subjected to hardness measurements (between 8 and 10 measurement points).

The surface hardness was measured at a load of 5 daN and a stress time of 15 s, using the Vickers HVS -10A apparatus. The histogram of their hardness values as well as those performed on the base metal is presented in Figure 3.1.

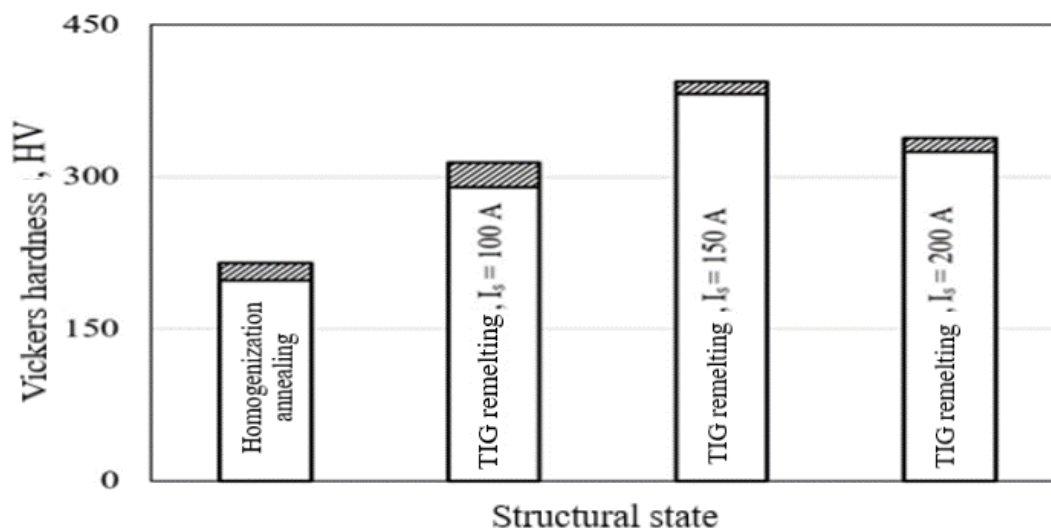


**Figure 3.1** Hardness histogram of base metal and locally remelted WIG samples

Figure 3.2 a,b,c shows the microstructure of the surface remelted locally by the TIG technique using three values of the current, respectively of the linear energy induced in the material:

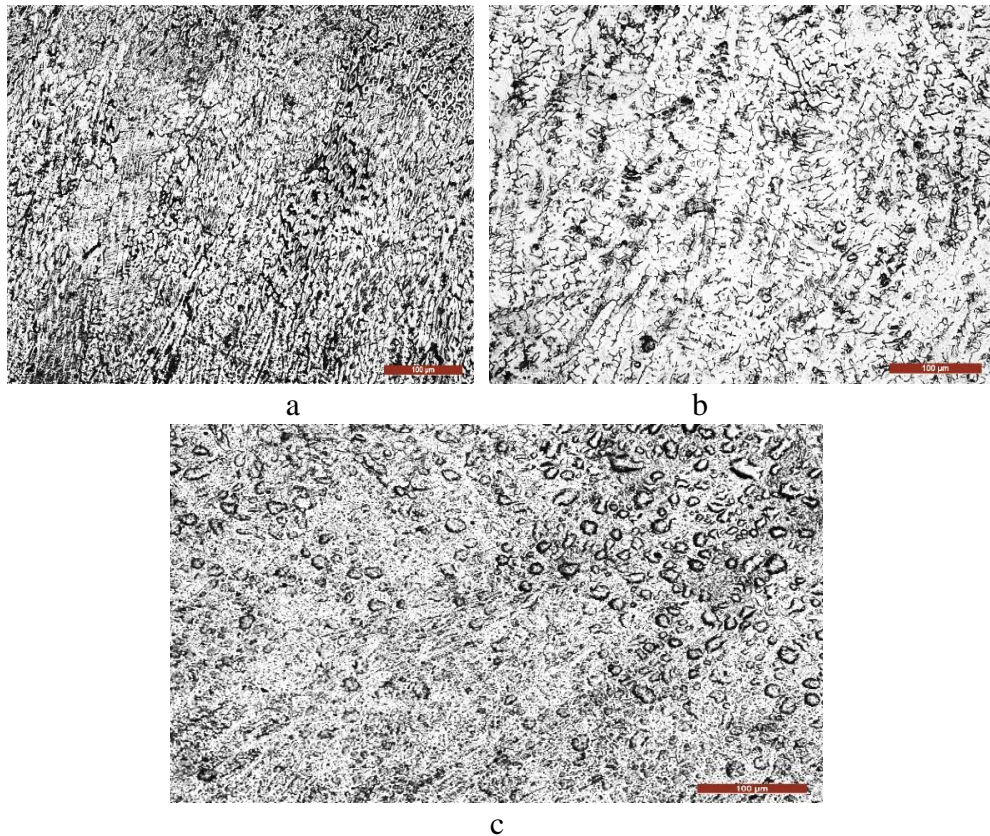


**Figure 3.2** MO x 200, Microstructure of the remelted surface a-  $I_s = 100$  A; b-  $I_s = 200$  A; c-  $I_s = 150$  A

For values of the remelting current of 150 A, respectively values of the linear energy of 6630 J/cm (Figure 3.2 c), the most favorable hardening situation appears both by finishing the granulation and by forming a solid solution

Figure 3.3 compares the specific MDE(t) curves for the four structural states, using as experimental values the algebraic averages of the values obtained on the sets of three samples.

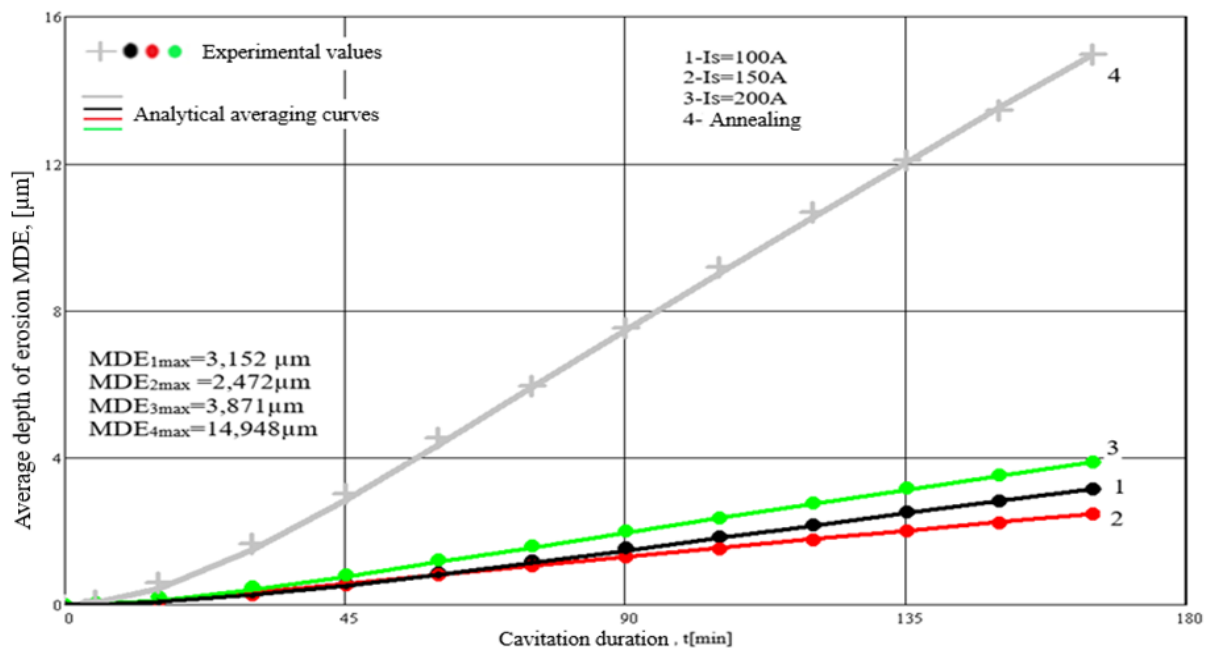


**Figure 3.3** Variation of the average depth of erosion, MDE, with the duration of the cavitation attack 1 – remelting with  $I_s = 100$  A; 2 – remelting with  $I_s = 150$  A; 3 – remelting with  $I_s = 200$  A, 4 – annealed state;

## Conclusions

Surface modification of high-alloy steel GX40CrNiSi25-20 using the TIG remelting technique at current intensities of 100–200 A leads to a significant improvement in cavitation erosion resistance.

The experimental results demonstrated that for melting current values of 150 A, the total cumulative mass loss ( $M_{tot} = 3,78$  mg) decreases more than 6 times compared to the initial state (without melting,  $M_{tot} = 22,89$  mg), and the erosion speed, according to the value towards which the curve  $v(t)$  tends to stabilize, decreases by approximately 5 times. Thus, the erosion rate,  $v_s = 0,145$  mg/min. for the initial unmelted surface and  $v_s = 0,023$  mg/min. for the melted surface TIG at  $I_s = 150$  A.

Local remelting through the TIG process of the surface of the investigated alloy samples causes an increase in hardness from values of approx. 200 – 210 HV at values of approx. 380 – 390 HV, depending on the current, respectively the linear energy introduced into the samples. The increase in hardness contributes significantly to the improvement of resistance to cavitation erosion.

The surface with the highest resistance to the erosion of vibrating cavitation has the one for which the current intensity is 150 A, respectively the linear energy is 6300 J/cm.

Compared to the homogenization annealing condition, the TIG surface modification technique causes an increase in the cavitation stress resistance from 3,86 times to 6,85 times after the values of cumulative average depths,  $MD_{E_{max}}$ , respectively from 3,84 times to 6,4 times, according to the values of the average rate of penetration of erosion,  $MD_{ERs}$

Scanning electron microscope investigations demonstrated that as a result of fatigue processes and plastic deformation effects, microcracks were initiated and developed at the triple contact points on the  $\gamma$  solid solution grain boundaries.

Following the coalescence of microcracks, material removal occurred during cavitation erosion. For values of the linear energy of 6300 J/cm, the degradation of the surface is more uniform, the depth of the microcraters formed as a result of the removal of chemical combination phases from the grain boundaries reaches values of 15  $\mu\text{m}$ , while in the austenite matrix the depth does not exceed 10  $\mu\text{m}$ . Conversely, at lower values of the linear energy (4080 J/cm), or at too high values of it (8880 J/cm), the maximum depths of the microcraters exceed 24  $\mu\text{m}$ .

## Cap.4 Process parameters, microstructure and cavitation erosion behavior of laser remelted GX40CrNiSi25-20 steel surface layers

Technological variants of laser beam surface treatment (local remelting, martensitic hardening, alloying, etc.) contribute to improving the mechanical properties and resistance to cavitation erosion of many ferrous alloys [153 - 164]. Gadag S.P. et al [147], Dube D. et al. [44], obtained an increase in the cavitation erosion resistance of nodular graphite cast iron and steel by laser beam remelting of the surfaces. Kwok et al conducted similar research on local laser beam remelting of stainless steel and laser alloying of various alloy surfaces [35][100]. Tang C.H, Cheng F.T and Man H.C. have proven that by laser remelting the surface of Cu-based alloys an improvement in cavitation erosion resistance is obtained [164].

The main objective pursued in this chapter aims to increase the resistance to cavitation erosion by obtaining a fine-grained microstructure in the surface layer, without changing the chemical composition of the base material. During the remelting process, some of the absorbed thermal energy penetrates the material, which results in the generation of a high temperature gradient between the liquid layer and the underlying solid [17][35][54].

The installation used is of the Trumpf Trucell 7040 type, powered by the Trudisk 4002 Yb-YAG laser source with a quality laser beam of 8mm\*mrad, wavelength, 1030 nm. By means of a Brightline optical fiber with a diameter of 200  $\mu\text{m}$ , the installation was programmed for this application with the help of the Trutops software provided by the Trumpf company. The optical module for projecting the laser beam onto the workpiece is mounted

on 2 numerically controlled linear axes and also contains 3 mirrors: collimation, reflection and focusing, arranged on 2 more axes of rotation and one of translation. The protective gas used was argon, whose flow rate was 10 l/min. The distance between the nozzle and the surface of the sample in the material to be processed was 16 mm. The advance speed was the variable parameter, having the values: 0,8 m/min., 1 m/min., and 1,2 m/min. The width of the fused material tracks was 0,9 – 1 mm, their degree of overlap was 50%, and their depth was 0,4 – 0,6 mm.

Once the programming is completed and the sample is fixed in the device, the actual melting process is triggered which is fully automated. When the optical module reaches the start position, the laser beam with the power of 1000 W and the frequency of 5010 Hz is triggered in a point projection, 1 mm in diameter on the sample to be processed, where an energy density of 1273 W/mm<sup>2</sup> is recorded.

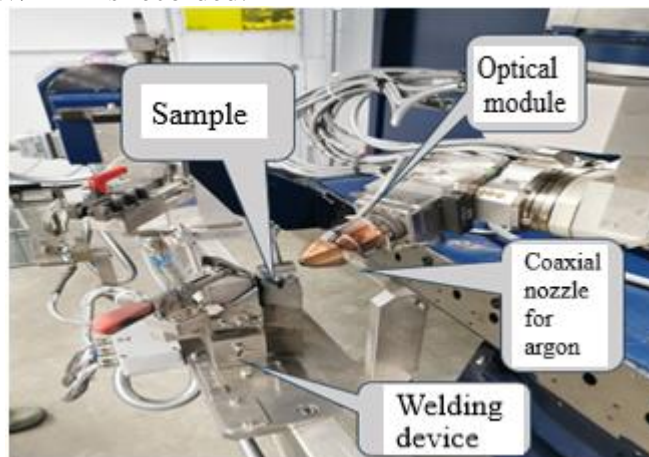


**Figure 4.1** Laser beam remelting equipment

The hardness on the remelted surface was measured at a load of 50 N and a stress time of 15 s, using the Vickers HVS -10A apparatus.

The remelted surfaces with the 3 values of the advance speed were processed by grinding - polishing operations and then subjected to hardness measurements (between 8 and 10 measurement points). The histogram of their hardness values as well as those performed on the reference material is shown in Figure 4.2.

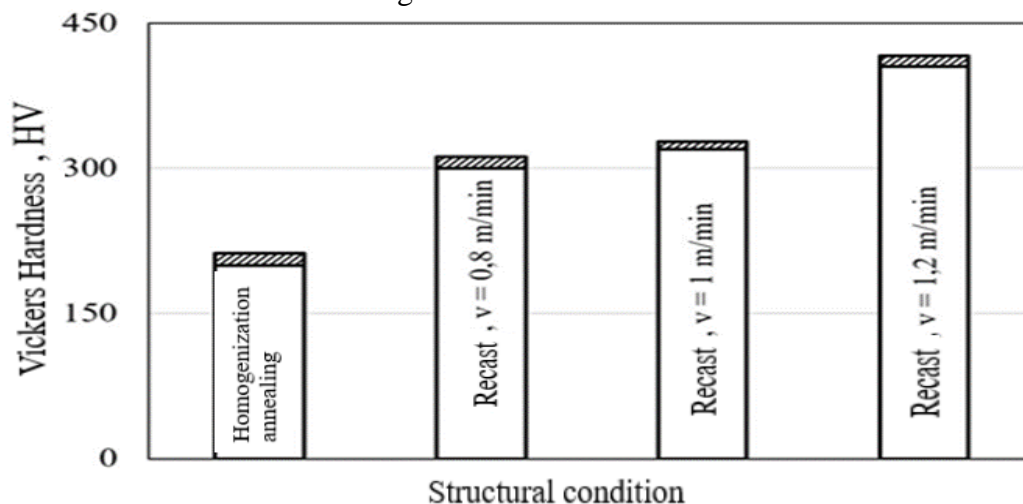
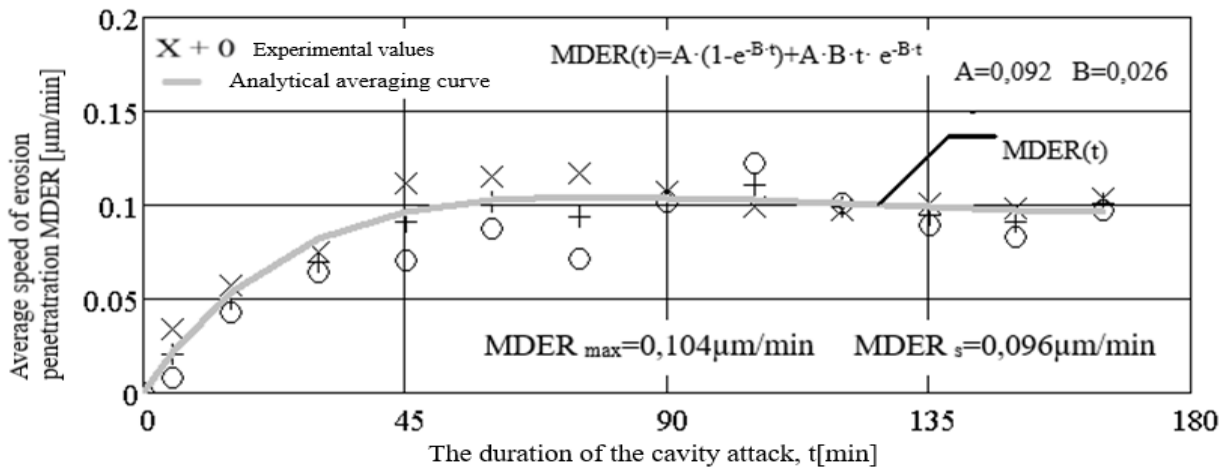
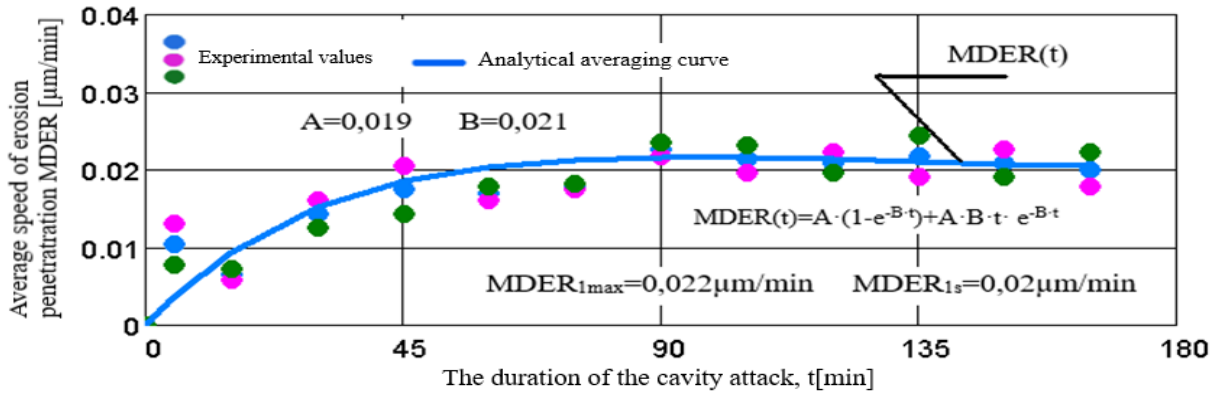


**Figure 4.2** Hardness histogram of base material and locally remelted Yb -YAG samples

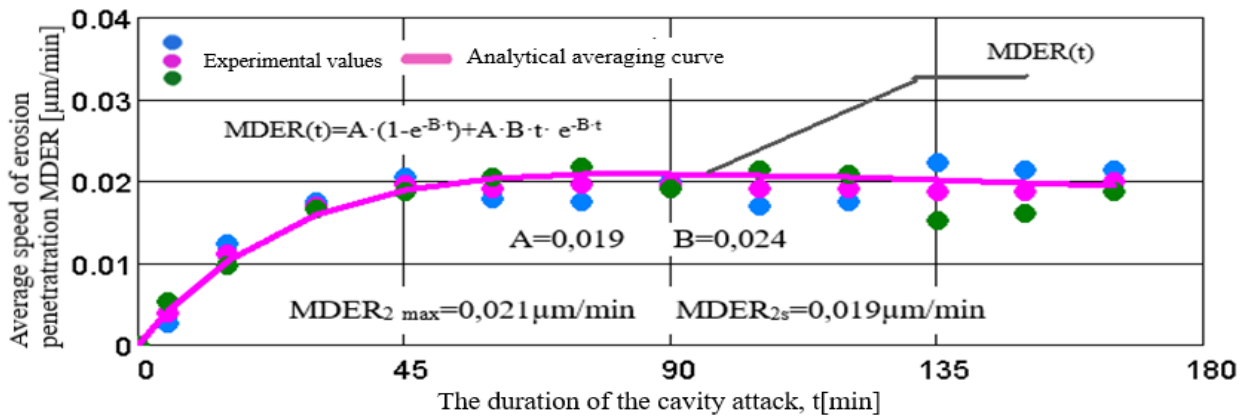
Thus, if in the annealed state the hardness values are approx. 210 HV, after laser remelting, values of up to approx. 400 HV. The diagrams shown in Figure 4.3 show the experimental values of the average erosion penetration velocities, related to the intermediate cavitation intervals and the MDER(t) averaging curves.



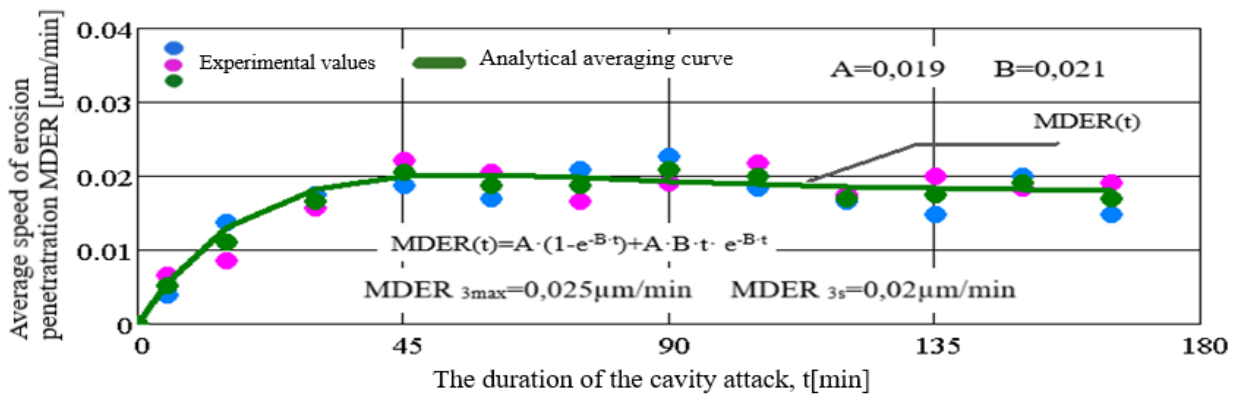
-a- annealed state



-b- laser remelted state with speed  $v = 0.8 \text{ m}/\text{min}$



-c- laser remelted state with speed  $v = 1 \text{ m}/\text{min}$



-d- laser remelted state with speed  $v = 1,2 \text{ m}/\text{min}$

**Figure 4.3** Variation of average erosion penetration speed with duration of cavitation stress

In the graphs in Figure 4.4 and Figure 4.5, the specific MDE(t) and MDER(t) curves are presented comparatively, for the four structural states.

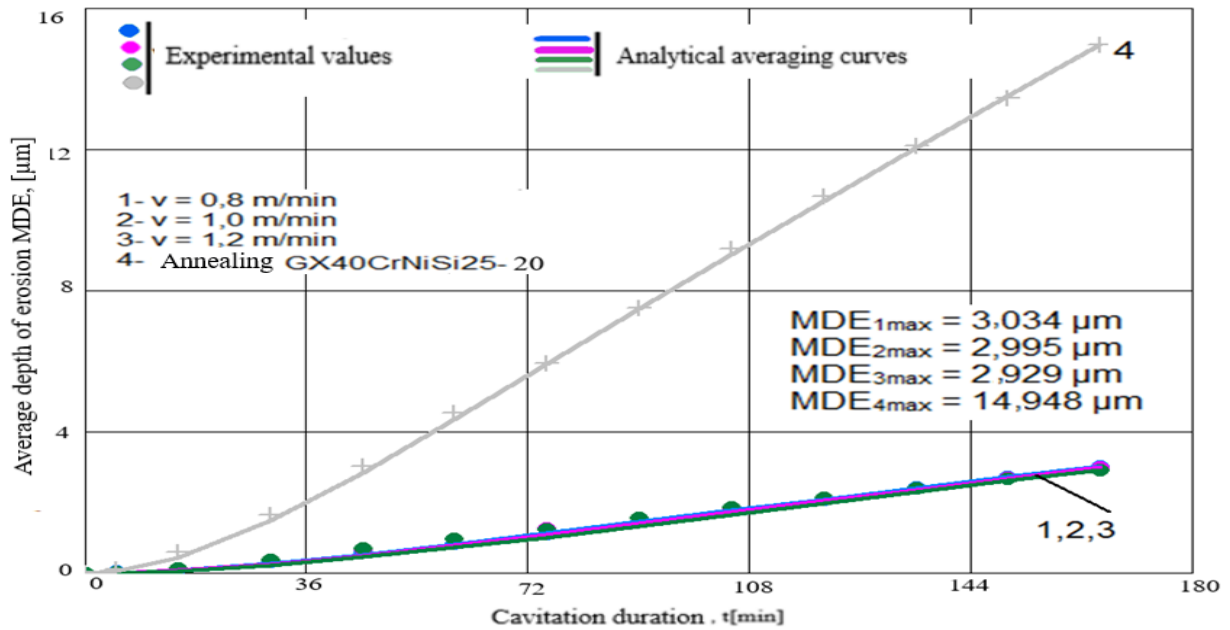


**Figure 4.4** Variation of the average erosion depth, MDE, with the duration of the cavitation attack: 1 – remelting with  $v = 0.8\text{m/min}$ , 2- remelting with  $v = 1\text{m/min}$ , 3- remelting with  $v = 1.2\text{m/min}$ , 4 – annealed state

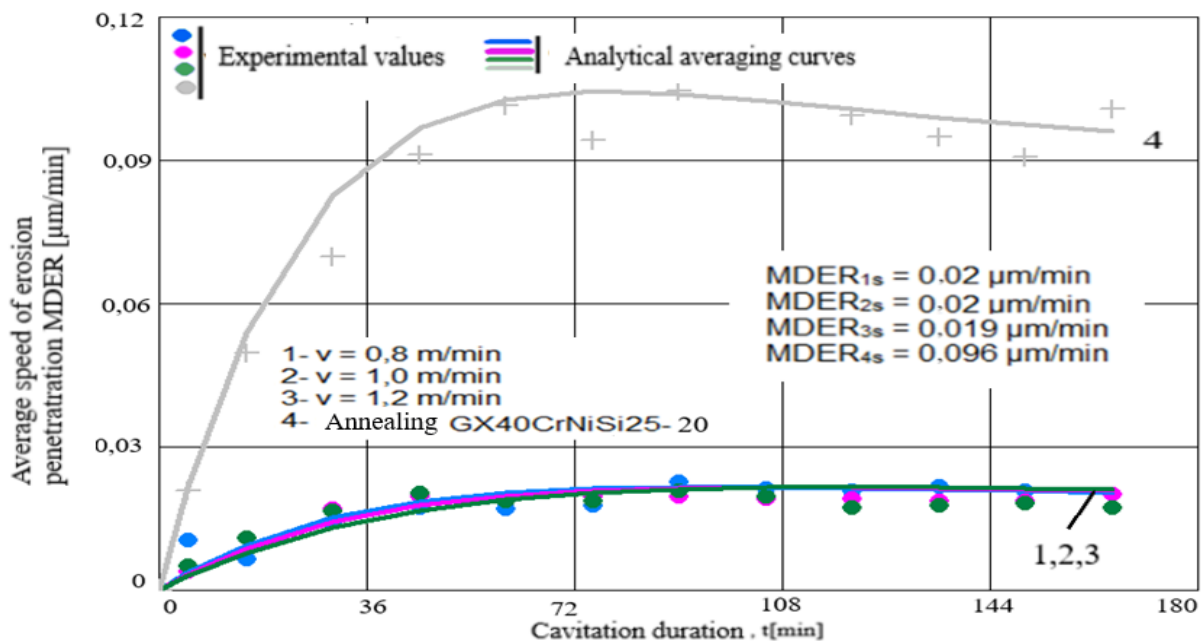


**Figure 4.5** Variation of the average speed of the erosion penetration depth, MDER, with the duration of the cavitation attack, 1- remelting with  $v = 0,8\text{m/min}$ ., 2 - remelting with  $v = 1\text{m/min}$ ., 3 - remelting with  $v = 1,2\text{m/min}$ ., 4 – annealed state

### Conclusion

The local remelting by the laser process of the surface of the samples from the investigated alloy is manifested by an increase in hardness from values of approx. 200 – 210 HV (annealed state) at values of approx. 380 – 390 HV, depending on the linear energy introduced into the material. The increase in hardness contributes significantly to the improvement of resistance to cavitation erosion.

The surface with the highest resistance to vibrating cavitation erosion has the one for which the melting laser speed is  $v = 1,2\text{m/min}$ . The increase in resistance, compared to the other two regimes, is:

- according to the value of the MD<sub>E</sub>max parameter, the increase achieved is 2,2% compared to the regime with  $v = 1\text{m/min}$  and 3,5% compared to the structure obtained by using the laser melting speed  $v = 0,8\text{m/min}$
- according to the value of the MD<sub>E</sub>R<sub>s</sub> parameter, the increase achieved is 5,2% compared to the structure obtained by using laser melting speeds,  $v = 0,8\text{m/min}$ . and  $v = 1\text{m/min}$ .
- compared to the initial reference state of the material, the laser surface modification technique produces an increase in the resistance to cavitation stresses from 4,9 times to 5,1 times after the cumulative average depth values, MD<sub>E</sub>max , respectively from 4,8 times up to 5 times, according to the average erosion penetration rate values, MD<sub>E</sub>R<sub>s</sub>.

### Cap. 5 Microstructure and resistance to cavitation of layers deposited by welding in manganese austenitic alloy

Deposited layers of manganese austenitic alloys are known for high impact wear resistance caused by rapid cold strain hardening [137]. Due to the low yield strength of these alloys, they can be extensively deformed before cold strain hardening becomes effective [133]. The resulting microstructure consists of a strain-induced martensite that can have a volume-centered cubic or compact hexagonal crystal lattice, known as  $\alpha'$  and  $\epsilon$  martensite, respectively [137][179].

It is mentioned that according to the knowledge of the author of the doctoral thesis, no research has been carried out regarding the process of hard coating of austenitic stainless steels cast in pieces, with electrodes of manganese austenitic alloys using a special technique of manual electric arc welding, namely, the which uses pulsed current.

The aim pursued in this chapter is to present a new processing route for the development of reasonable cost layers from manganese austenitic alloys.

The basic material that is the object of the experimental research is cast stainless steel brand GX40CrNiSi25-20 (W.1.4848), EN 10295. As an additional material, the CITOMANGAN electrode with a basic coating of manganese austenitic steel, symbolized DIN 8555: ~E 7, was selected - UM - 200 KP, respectively EN 14700 : E Fe 9 which is recommended for depositing wear-resistant layers in conditions of strong impacts and shocks. The experimental research aimed to make depositions by welding with electrode wrapped in one, two, respectively in three layers on the front surface of cylindrical samples  $\Phi 20 \times 25\text{mm}$ . As an absolute novelty in this respect, it was proposed for manual welding with covered electrode, in pulsed current, the use of a universal MAGIC WAVE 300 welding source from the Fronius company, which allows, as a variant, TIG welding in pulsed current, figure 5.1.

The welding source used in the present case allows a very wide range of modification of these parameters both in terms of frequency and pulse time - base time. This fact is a great advantage when it comes to the stability of the electric arc and the control of the linear energy introduced into the part.



Figure 5.1 MAGIC WAVE 300 welding rig

The novelty consists in the fact that in the welding head of the TIG torch, in its tweezers, instead of the non-fusible tungsten electrode, a covered electrode, intended for hard loading, was fixed, Figure.5.2.

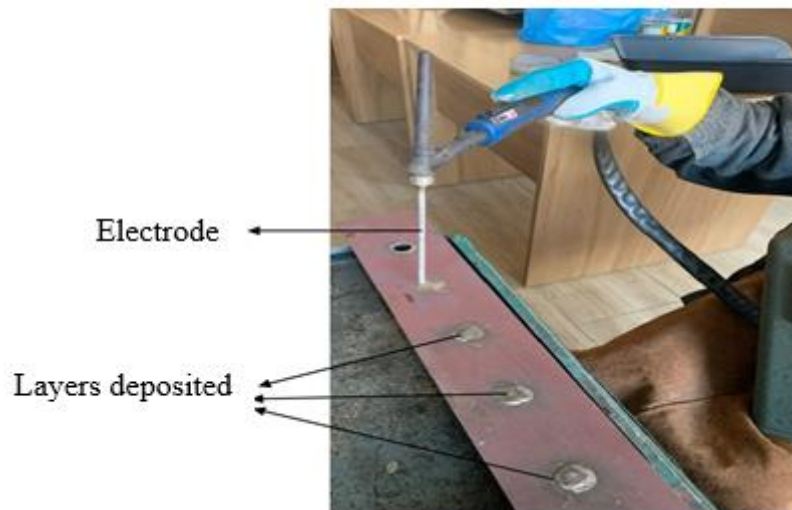


**Figure 5.2** TIG welding head with coated electrode

Also in this sense, the samples were fixed (embedded) in a carbon steel plate with the dimensions  $L \times w \times h = 400 \times 70 \times 10$  mm, primarily to avoid material leakage on the circumference of the samples and the formation of appropriate deposits, but also for to prevent the movement of the samples during welding, given their small dimensions.

The entire assembly was mounted on a box filled with water, so that an important part of the mass of the samples was forced to be cooled with water during welding, avoiding their heating as much as possible, which is the basis of the research approach. In order to maintain a constant water temperature, during welding, it was continuously refreshed through an open circuit flow system.

The welding was followed as previously shown by the achievement of plastic deformation by hammering with a pneumatic chisel. It is observed that the deposition of the material is uniform, without unevenness, without leakage of material, without concavities or convexities, with a final crater reduced in size, without surface macro-defects or with reduced splashes.

After cooling the samples to room temperature, the second and third layers were successively made, followed by the related hammering and the visual control of the surfaces.

Figure 5.3 shows the surface appearance of the loaded and plastically deformed samples after welding.

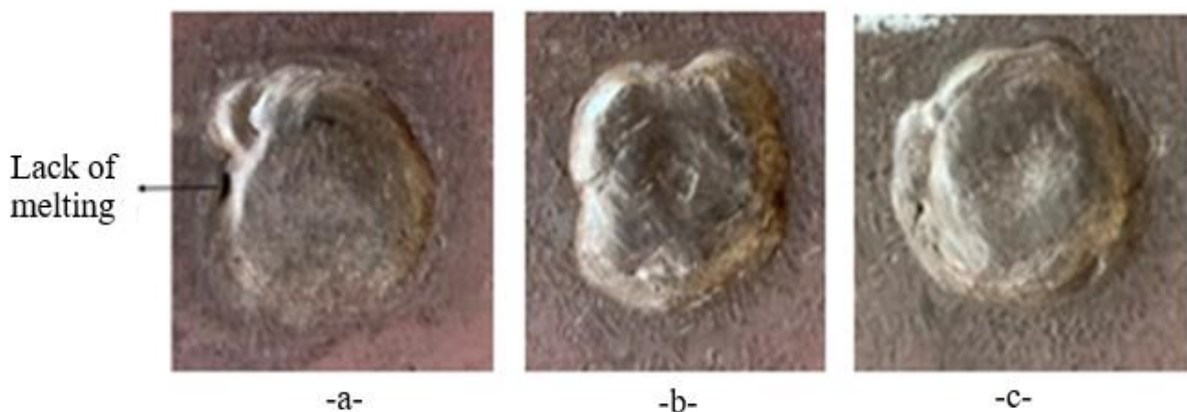


**Figure 5.3** The macroscopic appearance of the deposits: a – with 1 layer; b – 2 layers; c – 3 layers

In the single-layer sample, a lack of melting between the sample and the support is observed, attesting that the deposition minimally affects the support metal.

This defect apparently does not constitute an impediment considering that the diameter of the sample to be welded is greater than the diameter of the finished sample after mechanical processing.

It is mentioned that the welded samples can be detached from the support material by acting with a pressing force exerted by a press or by cutting with a laser beam a round of dimensions 2-3 mm larger than the diameter of the sample, following as later, at mechanical processing, this surplus should be easily removed by chipping. The hardness tests were carried out on a Vickers HVS -10A machine, at a load of 50 N and a stress time of 15 s. They showed that for the experimental conditions used, values of 186 - 219 HV5 are obtained in the deposited layer not mechanically cross-grained and of 468 – 492 HV5 following mechanical hardening.

The results of the macro-graphic investigations carried out on the samples taken perpendicular to the longitudinal axis of the deposited layers prove that they do not present defects of metallic continuity of the type of lack of penetration or lack of melting between the passes, of the pores or the cracks and crevices.

X-ray energy dispersion analyzes highlight the fact that along with the change in Fe content, there are important changes in Ni, Cr and Mn contents in the first layer deposited in the microzone near the base metal.

### Comparison between the 3 samples coated with manganese austenitic steel and comparison with the initial steel GX40CrNiSi25-20 in the annealed state

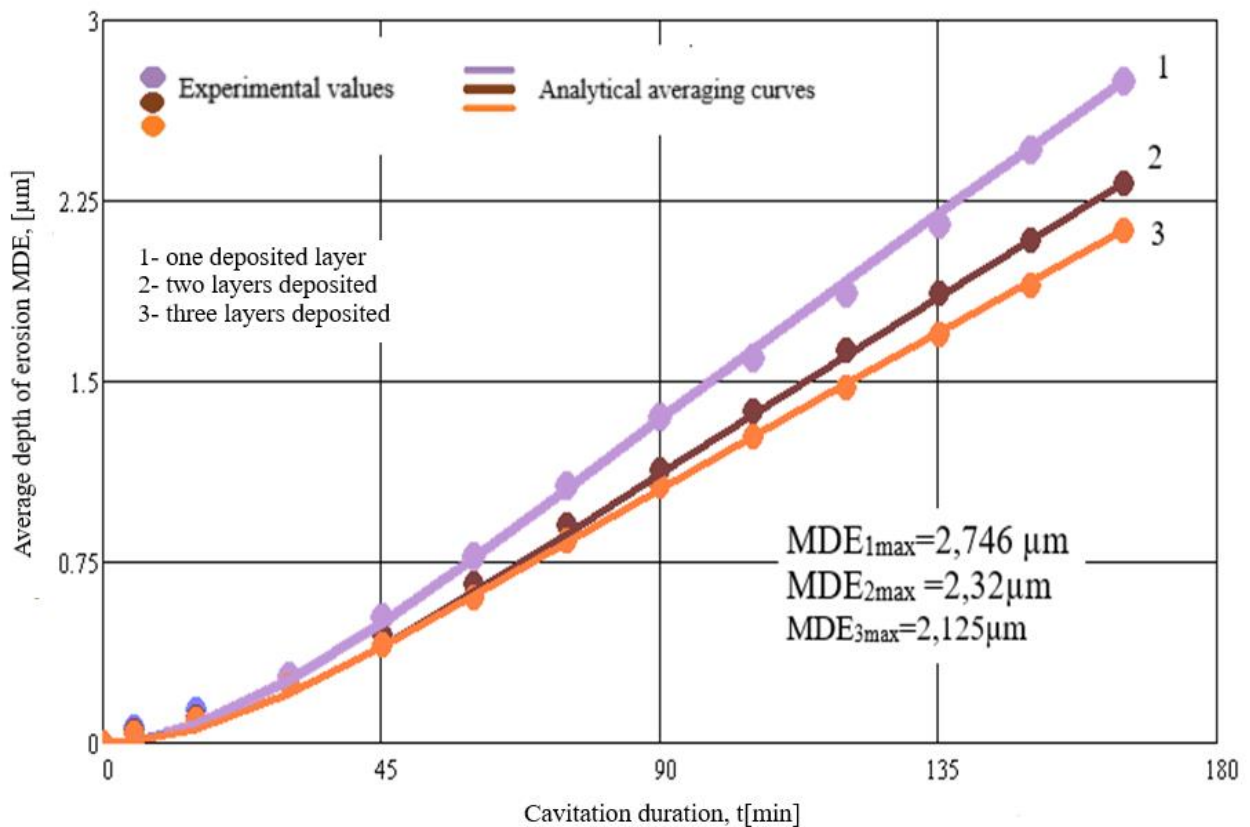


**Figure 5.4** Evolution of the average depth of erosion MDE with attack time, for the three sets of samples coated with manganese austenitic steel

The three-layer samples have the most homogeneous behavior, the experimental values being located approximately on the averaging curves.

This aspect suggests that the losses in the intermediate durations are with small differences, and denotes that the microstructure of the three-layer samples is finer, with grains that have small dimensional and mass differences between them;

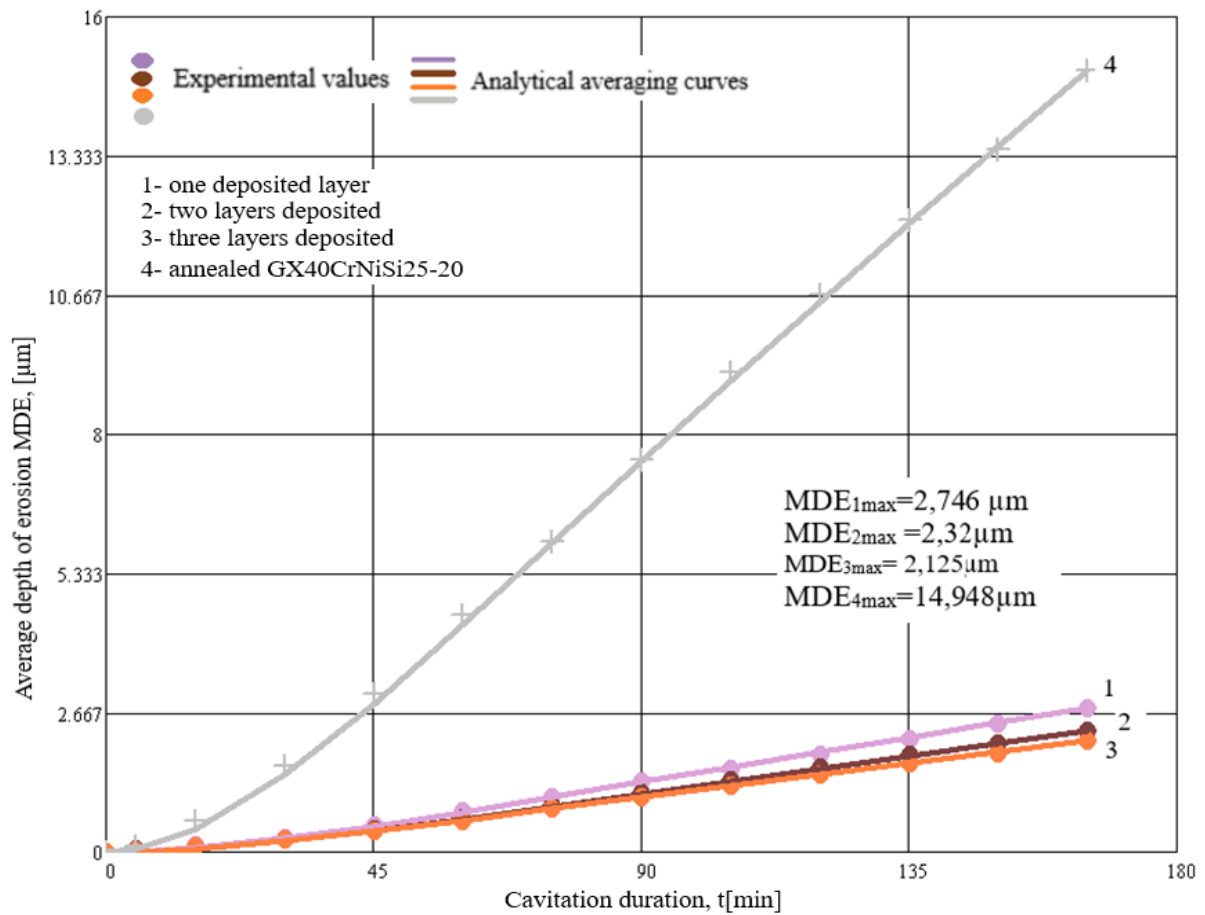


**Figure 5.5** Variation of the mean depth of erosion, MDE, with the duration of the cavitation attack for the reference material and for the three sets of samples with deposited metal

The data in the diagrams shown in Figure 5.4 and Figure 5.5 show that the behavior and resistance to cavitation of surfaces with one, two or three layers deposited by TIG welding are superior to the structure of the base metal obtained by annealing.

The dispersion of the points suggests that the microstructures of the three types of samples are finer, more homogeneous and with mechanical properties (especially hardness) superior to the annealed state.

The increase in strength, achieved compared to the annealed state, using the values of the  $M_{tot}$  and  $MDE_{max}$  parameters, is about 5.4 times for the samples with one layer deposited, about 6.4 times for the samples with two layers deposited and about 7 times for the samples with three layers deposited.

### Conclusions

The process of loading by manual welding with a covered electrode, in pulsed current, using a manganese austenitic alloy as an additive material, ensures a good metallurgical connection layer - substrate because it allows a very precise dosage of the energy introduced into the two components of the system.

The microstructure of the deposited metal consists of an austenite matrix with carbide precipitates. After hardening by cold deformation, a fragmentation of the dendritic structure occurs with the formation of macles or  $\epsilon$  martensite and preferentially precipitated carbides. The results of the cavitation test show that among the types of samples with deposited layers, the three-layer ones have the highest resistance to cavitation, from 9% to 33%, depending on the reference parameter.

Relative to the state of the base metal, with annealing heat treatment, the strength increases obtained by metal deposition, regardless of the number of layers, are very high, from 5 times to 7 times.

## Cap. 6 Final conclusions and original contributions. New research directions

### Final conclusions and original contributions

1. To reduce the negative impact of erosion on machine components, there are numerous methods of increasing the resistance to cavitation erosion, such as: thermal and thermochemical treatments, application of coatings, local remelting of the surface, etc.
2. The response of metal alloys to cavitation attack is indicated to be done both by measuring the mass loss as a function of the cavitation time and by analyzing the damaged surfaces with the help of optical microscopy, scanning electron microscopy and X-ray diffraction.
3. The heat treatment of annealing for homogenization applied to cast steel GX40CrNiSi25-20 manifests itself by increasing the cavitation resistance by about 1,8 times after the maximum value of the cumulative average depth of erosion, MDE, respectively by about 1,7 times after the values towards which the erosion rate parameter, MDER, is stabilized compared to the GX10Cr13 steel considered as a benchmark.
4. The physical modification of the surface of the high-alloy steel GX40CrNiSi25-20 using the TIG remelting technique at a current intensity of 150 A, respectively a linear energy of 6300 J/cm leads to an increase in hardness from values of approx. 200 – 210 HV at values of approx. 380 – 390 HV. This causes a decrease in the erosion rate of about 5 times compared to the homogenization annealing condition applied to the reference material.
5. X-ray diffraction analyzes proved that both the microstructure of the reference metal and the remelted layer on the surface is constituted by the solid solution  $\gamma$  (austenite) and carbides of the type M<sub>7</sub>C<sub>3</sub>, M<sub>23</sub>C<sub>6</sub>.
6. For values of the linear energy of 6300 J/cm, the degradation of the surface is uniform, the depth of the micro-craters formed as a result of the removal of chemical combination phases from the grain boundaries reaches values of 15  $\mu\text{m}$ , while in the austenite matrix the depth does not exceed 10  $\mu\text{m}$ . Conversely, at lower values of the linear energy (4080 J/cm), or at too high values of it (8880 J/cm), the maximum depths of the micro-craters exceed 24  $\mu\text{m}$ .
7. Compared to the reference state of the material, the laser surface modification technique causes an increase in the resistance to cavitation stresses from 4,9 times to 5,1 times after the values of cumulative average depths, MD<sub>E</sub>max, respectively from 4, 8 times to 5 times the average erosion penetration rate values, MDERs.
8. The micro-fractographic investigations carried out on the surfaces tested for cavitation for 165 min. demonstrated that the initiation of erosion occurs on the boundaries of the austenite grains by the removal of carbide particles, after which an extension of this phenomenon is found inside these grains.
9. As a result of the high fragility of the eutectic carbide particles in the reference metal, the craters formed as a result of their expulsion and the partial or complete pulling out of some crystalline grains are much deeper (more than 32  $\mu\text{m}$ ), compared to those resulting from erosion of the remelted surface (maximum depth does not exceed 9  $\mu\text{m}$ ).
10. Microscopic examination of cross sections through surface layers that were remelted and cavitation tested for 165 min. proves that the laser process is manifested by the accentuated finishing of the granulation and carbide particles precipitated both from the liquid phase and from the austenite.

11. The relatively high advance speeds of the laser beam make the thermal cycle faster, the degree of undercooling higher, the critical radius of the crystallization seed smaller and the resulting microscopic structure finer. Or, the finer the granulation, the higher the resistance to dynamic shock stresses generated by cavitation bubbles and implicitly the higher the resistance to cavitation erosion.

12. The process of loading by manual welding with covered electrode in pulsed current using a manganese austenitic alloy as an additive material allows a precise dosage of the energy introduced into the two components of the system, with favorable effects on the finish of the granulation and the microstructure of the deposited layer.

13. The high degree of alloying of the base material and the additive, as well as the use of pulsed current in the hard coating process, justify the low dilution values.

14. After hardening by cold deformation, a fragmentation of the dendritic structure occurs with the formation of macles or martensite  $\epsilon$  and preferentially precipitated carbides.

15. The results of the cavitation tests show that compared to the structural state specific to the annealing for homogenization of the base metal, the strength increases obtained after welding deposition are 5-7 times.

### **New research directions**

Based on the research carried out in the doctoral thesis, the results obtained and presented in the paper, the following perspectives can be formulated for future research:

1. The development of new surface coating methods, for example thermal spraying, the PVD - physical vapor deposition and CVD - chemical vapor deposition processes and new thermal and thermochemical treatment technologies to improve resistance to cavitation erosion

2. Research of the structural degradation of these categories of metal alloys during the early phase of cavitation.

## Bibliography (selective)

6. Abouel-Kasem, A., Ezz El-Deen, A., Emara, K.M. and Ahmed S.M. : 2009, Investigation Into Cavitation Erosion Pits. *Journal of Tribology*, 131, 31605-031612
12. Annual Book of ASTM Standards (2010) Section 3: metals test methods and analytical procedures, vol 03.02. Annual Book of ASTM Standards, West Conshohocken, pp 94– 109
13. ASTM G32—2016. Standard test method for cavitation erosion using vibratory apparatus
17. B.K. Sreedhar, S.K. Albert, A.B. Pandit: Cavitation damage: theory and measurements – a review. *Wear*, 372–373 (2017), pp. 177-196
21. Berchiche, N. A.; Franc, J. - P. and Michel, J. M.: 2002, A cavitation erosion model for ductile materials. *Journal of Fluids Engineering*, 124(3), pp. 601–606 between cavitation erosion and corrosion of Monel K500 alloy in 3.5 wt% NaCl solution. *Materials Characterization*, Vol. 205, November 2023, 113340
22. Binder, W. O. Şi Spendelow, H. R., *Trans. Am. Soc. Met.*, vol. 43, 1951, p. 759
23. Bordeasu I. : Monografia Laboratorului de Cercetare a Eroziunii prin Cavitate al Universitatii Politehnica Timisoara (1960-2020). Editura Politehnica, Timișoara, Romania, 2020
27. Bordeășu I.: Eroziunea cavitațională a materialelor. Editura Politehnica, Timișoara, 2006
28. Bordeășu, I., *Distrugerii cavitaționale*, Editura MicroSOFT, Timișoara, 1998.
29. Bordeășu, I.; Patrascoiu, C.; Badarau, R.; Sucitu, L.; Popoviciu, M.; Balasoiu, V. New contributions in cavitation erosion curves modeling. *FME Trans.* 2006, 34, 39–43.
35. C.T. Kwok, H.C. Man, F.T. Cheng, K.H. Lo: Developments in laser-based surface engineering processes: with particular reference to protection against cavitation erosion. *Surf. Coat. Technol.*, 291 (2016), pp. 189-204
37. Chahine, G. L., Franc, J.-P. and Karimi, A., “Laboratory Testing Methods of Cavitation Erosion”, in Kim, K.-H. et al. (eds.), *Advanced Experimental and Numerical Techniques for Cavitation Erosion Prediction, Fluid Mechanics and Its Applications* 106, Springer Science+Business Media Dordrecht 2014
- 41 .Choi, J.-K., Jayaprakash, A. and Chahine, G. L.: 2012, Scaling of Cavitation Erosion Progression with Cavitation Intensity and Cavitation. *Wear*, pp. 278–279, 53–61
43. Cosma (Alexa), I. Mitelea, I. Bordeasu, V. Alexa, C.M. Craciunescu : Cavitation erosion resistance of GX40CrNiSi 25 – 20 cast stainless steel. *Proceedings International Conference on Metallurgy and Materials*, Brno Czech Republic, ISBN 978-80-87294-99-4, ISSN2694-9296. *Metal.2021.4136*, 514-519
44. D. Dube, M. Fiset, R. Laliberte, R. Simoneau: Cavitation resistance improvement of IRECA steel via laser processing. *Material Letters*, Vol. 28, September 1996, pp. 93-99
47. Da Silva F.J., a.o.: Cavitation erosion behavior of ion – nitrided 34CrAlNi7 steel with different microstructures. *Wear*, Vol.304, Iss.1-2, 2013, pp. 183 – 190
48. Di Vernieri Cupparia, M.G., Wischnowski, F., Tanaka, D.K., Sinatora, A.: Correlation between microstructure and cavitation–erosion resistance of high–chromium cast steel – Preliminary results. *Wear*, 1999, Vol. 225–229, Part.1, pp. 517–522
52. Espitia A.L., Toro A.: „Cavitation resistance, microstructure and surface topography of materials used for hydraulic components”, *Tribology International*, Vol. 43, pp. 2037–2045, 2010
54. Franc J.-P. and Michel J.M.: *Fundamentals of cavitation*. Kluwer Academic Publishers-Dordrecht/Boston/London, 2004
56. Franc, J.P., s.a., *La Cavitation, Mecanismes physiques et aspects industriels*, Press Universitaires de Grenoble, 1995
57. Franc, J.-P.: 2009, Incubation Time and Cavitation Erosion Rate of Work-Hardening Materials. *Journal of Fluids Engineering*, 131(2), 021303-021317
58. Garcia, R., Hammitt, F.G., Nystrom, R.E., *Corelation of cavitation damagewith other material and fluid properties, Erosion by Cavitation or Impingement*, ASTM, STP 408 Atlantic City, 1960

61. Guiyan Gao, Zheng Zhang : Cavitation erosion mechanism of 2Cr13 stainless steel. *Wear*, Vol. 488–489, 15 January 2022, 204137
65. Hammitt, F.G., *Cavitation and Multiphase Flow Phenomena*, McGraw Hill International Book Company, 1980.
66. Hammitt, F.G., De M., He, J, Okada, T., Sun, B.H., Scale effects of cavitation including damage scale effects, Report No. UMICH, 014456 - 75 - I, Conf. Cavitation, Michigan, 1980 <http://go.microsoft.com/fwlink/p/?LinkId=255141>, pp.187
69. Haro S., Lopez D., Wong A., Martinez L., Velasco A., Viramontes R. : Aging of a Heat Resistant Alloy. 19th ASM Heat Treating Society Conference Proceedings Including Steel Heat Treating in the New Millennium, 2000, pp. 1 – 7
74. Heathcock și alții, *Wear*, vol. 81, 1982, p. 311
90. Jie-Hao Chen, Weite Wu : Cavitation erosion behavior of Inconel 690 alloy. *Materials Science and Engineering: A*, Vol. 489, Issues 1–2, 20 August 2008, pp. 451-456
97. Krella A.K., Krupa A.: Effect of cavitation intensity on degradation of X6CrNiTi18-10 stainless steel. *Wear* 408–409 (2018), pp. 180–189
98. Kwok C.T, H.C. Man, F.T. Cheng, K.H. Lo: Developments in laser-based surface engineering processes: with particular reference to protection against cavitation erosion. *Surf. Coat. Technol.* 291 (2016) pp.189–204
99. Kwok T.C.: „Cavitation erosion and pitting corrosion behaviour of laser surface – melted martensitic stainless steel UNS S42000”, *Surface and Coating Technology*, vol. 126, Iss. 2 – 3, pp. 238–255, 2000
100. Kwok, C.T., F.T. Cheng and H.C. Man : Synergistic effect of cavitation erosion and corrosion of various engineering alloys in 3.5% NaCl solution. *Materials Science and Engineering A*, 290(1-2): pp. 145 – 154, 2000
101. Kwook C., Man H., Cheng F.: Cavitation erosion and pitting corrosion of laser surface melted stainless steels. *Surface and Coatings Technology*, 99 (1998), pp. 295-304
102. Kwook C. T., Man H. C., Cheng F. T.: Cavitation erosion and damage mechanisms of alloys with duplex structures. *Materials Science and Engineering A* 242 (1998), pp. 108-120
114. Majid Abbasi, Mahdieh Vahdatnia, Ali Navaei : Solidification Microstructure of HK Heat Resistant Steel. *International Journal of Metalcasting/Volume 9, Issue 4, 2015*, pp. 14 – 26
116. Marcio Gustavo Di Vernieri Cupparia, Frank Wischnowski, Deniol K, Tanaka, Amilton Sinatora : Correlation between microstructure and cavitation–erosion resistance of highchromium cast steel—preliminary results. *Wear*, Vol. 225 – 229, Part.1, 1999, pp. 517 – 522
122. Mitelea I., Lugscheider E., Tillmann W., „Știința Materialelor în construcția de mașini”, Editura Sudura, Timișoara, România, pp. 430-431, 1999
126. Momeni S., Tillmann W., Pohl M.: Composite cavitation resistant PVD coatings based on NiTi thin films. *Materials and Design* 110 (2016), pp. 830-838
134. Pai R. and Hargreaves, D.J. : Performance of environment-friendly hydraulic fluids and material wear in cavitating conditions. *Wear*, 252, pp. 970–978, 2002
137. Pengjie Wang, Jiakuan Ren, Qiyuan Chen, Jun Chen, Zhenyu Liu : Effect of secondary twins on strain hardening behavior of a high manganese austenitic steel at 77 K by quasi in situ EBSD. *Materials Characterization*, Vol. 180, October 2021, 111428
147. S. P. Gadag, M. N. Srinivasan: Cavitation erosion of laser melted ductile iron. *Journal of Material Processing Technology* Vol. 51, no 1-4, 1995, pp. 150-163
152. Shuji Hattori, Morio Kishimoto : Prediction of cavitation erosion on stainless steel
153. Shuji Hattori, Ryohei Ishikura: Revision of cavitation erosion database and analysis of stainless steel data. *Wear* Volume 268, Issues 1-2, 4 January 2010, pp. 109-116
166. Thiruvengadam, A., *Cavitation erosion*, *Applied Mechanics*, Vol 24, Nr. 3, 1971
179. Xiaoyun Yuan, Liqing Chen, Yang Zhao, Hongshuang Di, Fuxian Zhu: Influence of annealing temperature on mechanical properties and microstructures of a high manganese austenitic steel. *Journal of Materials Processing Technology*. Vol. 217, March 2015, pp. 278-285

